Development of an ultrathin liquid sheet target for laser ion acceleration at high repetition rates in the kHz-range

M. Füle[1,2,3], A. P. Kovács[1,4],T. Gilinger[1], M. Karnok[1], P Gaál[1], S. Figul[5], G. Marowsky[5], K. Osvay[1,4]

1 National Laser-Initiated Transmutation Laboratory, University of Szeged, H-6720 Szeged, Hungary

2 Department of Experimental Physics, University of Szeged, H-6720 Szeged, Hungary

3 ELI ALPS, ELI-HU Non-Profit Ltd., Wolfgang Sandner utca 3., Szeged, H-6728, Hungary

4 Department of Optics and Quantum Electronics, University of Szeged, H-6720 Szeged, Hungary

5 Advanced Microfluidic Systems GmbH, Göttingen, Germany

email: mfule@titan.physx.u-szeged.hu, osvay@physx.u-szeged.hu

Abstract

A colliding microjet liquid sheet target system was developed, and tested for pairs of round nozzles of 10, 11, and 18μm in diameter. The sheet's position stability was found to be better than a few micrometers. Upon interaction with 50mJ laser pulses, the 18μm jet has a resonance amplitude of 16μm at a repetition rate of 33Hz, while towards 100Hz it converges to 10μm for all nozzles. A white-light interferometric system was developed to measure the liquid sheet thickness in the target chamber both in air and in vacuum, with a measurement range of 182 nm − 1μm and an accuracy of ±3%. The overall shape and 3D shape of the sheet follow the Hasson-Peck model in air. In vacuum versus air, the sheet gradually loses 10% of its thickness, so the thinnest sheet achieved was below 200nm at a vacuum level of 10^{-4}mbar, and remained stable for several hours of operation.

Keywords: nanometric liquid sheet targets; diagnostics; laser ion acceleration; vacuum test

I. Introduction

The most recent ultrashort pulse laser systems with an average optical power of hundreds watts and better than 2% stability [1-4] have laid the technological basis for the generation of stable, user-ready, high average power secondary systems, such as X-ray and gamma-ray sources. One of the major challenges of the utilization of high average power lasers in plasma physics and ion acceleration is the implementation of a high repetition rate, high density target system.

Since the 1990s, liquid-based target systems have been used for spectroscopical purposes at very low irradiation powers [5-12] mainly in ambient air, sometimes in vacuum. When a liquid target is to be illuminated by a high intensity laser with a peak intensity exceeding 10^{16} W/cm^2, the interaction must take place in vacuum, because of two reasons. First, the laser beam can significantly deteriorate already upon focusing due to nonlinear optical phenomena in ambient gases. Second, the generated X-ray radiation and particles, especially ions, are completely absorbed at pressures above a few torrs [13]. Hence, the first liquid targets for laser ion acceleration were typically droplets [14, 15], where the vacuum environment was relatively easy to keep, due to the low flowrate and the correspondingly low evaporation rate. Another approach to overcome vacuum issues was the development of cryogenic jets [16-18].

Following the first successful demonstration of a kHz-repetition rate proton accelerator based on a 0.5 μm ambient temperature liquid sheet [19], the development of various liquid target systems took off. Up to now, four different technologies have been developed to generate stable, thin liquid sheets in vacuum: one using the collision of two microjets [12], one using a 3D-printed nozzle [20], one using a gas-dynamic virtual nozzle (known as GDVN) [11] and one using isotropically etched glass nozzle [21]. It was shown that the ultimate laser repetition rate at which a liquid sheet can be operated is a few tens of kHz [22, 23]. Recently, few-micrometer thick liquid sheet targets have been developed for interaction with petawatt-class laser pulses, for ion acceleration [24-26] as well as for plasma mirror [22, 27].

The efficiency of whichon acceleration depends on the target thickness. According to the theories and experimental results, the sweet point lies in the submicrometer regime [28-31]. For few-cycle pulses, it is in the range of 100 nm [32, 33]. Hence, efficient ion

acceleration at a considerable repetition rate requires the development of a rapidly self-replenishing liquid sheet target of nanometric thickness in vacuum, and with sufficient position stability in the focal plane of the high intensity laser.

Several methods, most of them interferometric, have been implemented to measure the thickness of thin films from a few microns down to few tens of nanometers. To monitor the thickness change at different positions of the film, monochromatic interferometry has proven itself suitable [20, 25, 34-36]. When absolute thickness measurement is required, white-light interferometry (WLI) is the appropriate solution. Various WLI arrangements have been developed to record either the reflected [11, 20, 37] or the transmitted [21, 38-40] spectral interference from a given area of the film. One may regard the thickness measurement with coherent EUV as a special case of WLI, when an attosecond pulse train (APT) is produced in the liquid sheet target by high harmonic generation (HHG), and the thickness is determined from the modulation of the HHG spectrum arising from the time delay between the APTs [41].-According to the theory of WLI, the thinner the film, the broader the required spectral range [28].

White-light interferometric methods were successfully adopted for liquid sheets with thicknesses from submicron to several microns, mostly in ambient air [11, 12, 20, 21, 25, 34, 37-40]. It has been questioned since the first experiments in vacuum whether the thickness aligned and even measured in air is the same upon interaction in vacuum. The query has arisen both from experiments and theoretical considerations: upon closing and evacuating a vacuum interaction chamber, the mechanical and/or pressure impact, as well as the assumed change in surface tension due to cooling caused by the evaporation of the liquid may influence the liquid jet and hence the thickness of the sheet. To our knowledge so far two attempts have been made to measure or estimate the thickness of liquid sheets in vacuum. From their measurements, Galinis et al. [20] concluded that the thickness of sheets several microns thick is not affected in vacuum. This observation seems to contradict the estimate provided by Ekimova et al. [12]. They measured the evaporation loss in vacuum environment, and estimated that the thickness of the liquid sheet may decrease by 5% in vacuum. Hence, there is a need to investigate the effect of the vacuum pressure on the thickness of liquid sheets, especially of ultrathin ones. This calls for a special measurement scheme which is suitable for measuring thicknesses below 200 nm with high precision and which can be used in vacuum, too.

The liquid sheet formed by two microjets under a complicated flow dynamics is sensitive to the angle and position of the two jets [42, 43], the environmental vibrations [19], including the laser's repetition rate. If any disturbances occur, the jet may change position [23]. Hence, it is essential to investigate the position stability of the liquid sheet, which may then affect the stability of the interaction and eventually the secondary source generated (e.g. ions).

In this paper we report on the development and characterization of a nanometric liquid sheet target system based on colliding microjets. To the best of our knowledge, the 182 nm thick sheet we produced is the thinnest sheet so far. Moreover, this thickness was measured *in situ*, in the interaction chamber in ambient air, during evacuation, and also at the ultimate vacuum level in the 10^{-4} mbar regime, with the same optical arrangement. The sheet was demonstrated to be operational for more than three hours under vacuum conditions.

II.   The liquid jet system

The system consists of two main parts: the head with the nozzles (Fig. 1a) and the computer controlled liquid circulating system (Fig. 1b). Both parts were gradually developed to meet the two major requirements such as operation in high vacuum (10^{-4} mbar) and generating a flat and stable liquid target with a thickness well below one micrometer. Here we describe the final version of our system, avoiding details of the years-long development.
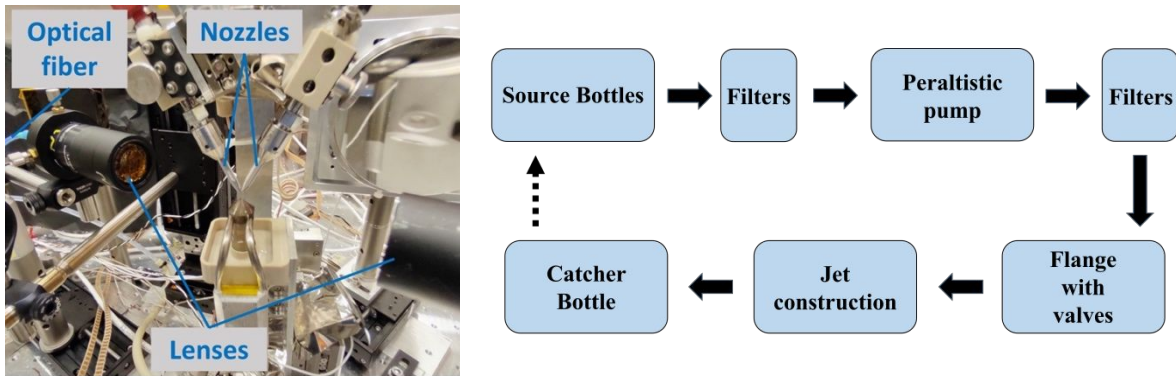

Figure 1 a) The liquid jet system: the two nozzles forming the sheet, and elements of the thickness measuring arrangement. i.e. the condensing and collimating lenses and the optical fiber and b) the logical diagram of the liquid jet circuit.

The flat liquid sheet is generated by two colliding cylindrical microjets, flowing from two identical, quartz nozzles (Fig. 2). At the inlet of the nozzle, the internal wall is parallel, and becomes tapered towards the tip of the nozzle, while its diameter decreases from approximately 0.5 mm to the orifice size of tens of micrometers. The slow parts of the parabolic flow profile close to the wall are cut off by the conus shaped inner channel before the tip, which results in a jet with laminar flow and a flat top flow profile. The size of this microjet is almost equal to the size of the orifice. The liquid sheet is formed upon the collision of these laminar flow microjets in the perpendicular plane with respect to the plane of the nozzles. The ultrathin liquid sheet is bordered by a few micrometer thick rim. The two sections of the rim meet again in a tip forming a second leaf in the perpendicular plane with respect to the first leaf. This sequence continues until liquid formation decays into droplets and spray. The sheet is the thickest near the meeting point, and the thinnest at the tip of the leaf-shaped liquid structure. The flowrate, the collision angle, the orifice size, and the properties of the liquid, especially its surface tension, determine not only the thickness, length, and width of a leaf, but also the number of consecutive leaves.

One may think that with the decrease of the orifice size, the liquid sheet would be made infinitesimally thin. However, there are a few practical limitations. First, the micromachining of a few-centimeter-long, mechanically stable capillary is exponentially challenging with a decreasing orifice diameter. Second, experience shows that micron-size particles start evolving in the liquid, which is hard to avoid. These particles originate partly from the air of the laboratory (ISO 8 optical cleanliness in our case), partly from the microparts of the liquid circulating system. Such tiny particles started blocking the orifices with a size below 15 μm, despite the applied finest liquid filters. The frequency of blocking events increased with smaller orifices. Hence, in our experiment, the smallest applied orifice diameter was 10 μm.

The impinging angle and the orifice diameter define the flowrate atwhich the leaf stability is satisfactory[11, 25]. We found that an impinging angle between 50° and 55° was suitable for all three microjets, running with water having a slight salinity (100 mg/l NaCl) in our experiments. The liquid sheet with orifice sizes of 10 μm, 11 μm, and 18 μm were stable within the flowrate ranges of 0.46−0.57 ml/min, 0.60−0.75 ml/min, and 1.28−1.32 ml/min, respectively. Under these conditions, the first, big leaf was followed by a second one only. The ratio of the lengths and widths of the leaves was about 4:1. Since the

characteristics of the two smallest liquid sheets we generated were very similar, for most of our discussions in the next sections we show the data for the smallest and largest nozzle orifices.

Proper design and control of the circulating system are essential for maintaining the sensitive conditions of the liquid leaf. A high-pressure pump system (*KNAUER Wissenschaftliche Geräte GmbH*) serves the common pipeline for the nozzle pair s. The pressure in the feeding pipe is adjusted between 60 to 90 bar depending on the flowrate and orifice size of the nozzles, and the cleanliness of the feeding system. To minimize pulsation in the pipe and consequently in the liquid microjets, a pulsation damping system is inserted right after the pumping head of the high-pressure pump. To guarantee long-term jet stability under vacuum conditions, a catcher system was designed to collect the liquid beneath the first liquid leaf and remove it from the vacuum environment. The catcher has a small heated orif6pprox.pprox. 100 ℃, ID: 500 μm) to prevent ice formation, and to allow us to drain the liquid into a bottle with a diaphragm pump. The bottle can be emptied without interrupting the jet or vacuum operation, which may make the liquid jet system operable infinitely (Fig. 1 b). In the current arrangement, however, the cold trap limits the operating time to ~10 hours. Namely, the vapor condenses on the surface of the cold trap filled with liquid nitrogen, and the accumulating ice layer decreases the efficiency of the cold trap. Depending on the flowrate and size of the leaf, the vacuum level increases after several hours, and breaks the operation.
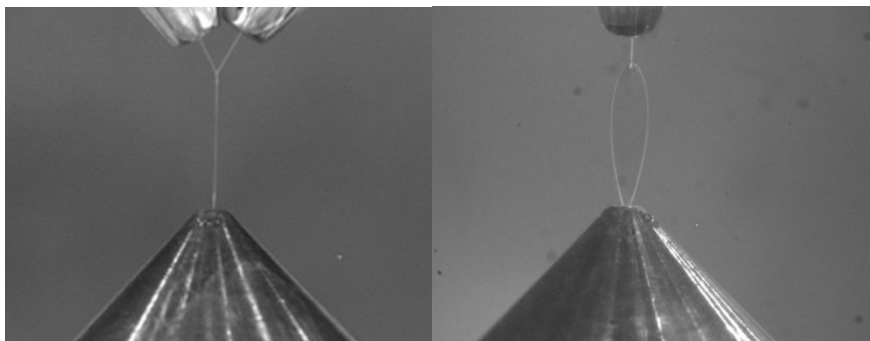

Figure 2. Formation of the top liquid leaf: a) side view, b) front view.

III.   Mechanical stability of the liquid sheet

Stochastic position stability

6

For long-term operation as an ion source, position stability is a must for any liquid phase target [44]. If the uncertainty of the target position is greater than the Rayleigh range of the focused laser beam, then the highly nonlinear laser-matter interaction results in a very unstable particle beam.

We placed a Micro-Epsilon® high precision distance measurement unit (ILD2300-20 type) against the liquid leaf target system in the normal direction to measure the position of the surface of the leaf. The readout frequency was 1.5 kHz, while the accuracy was 0.24 μm. We operated in the mid measurement range, roughly 5 cm away from the sheet; hence, the spot size was well below 100 μm on the center of each sheet. The liquid leaf position was then measured for five minutes at different flowrates. For illustration purposes, typical measurements are shown in Fig. 3. The stability of the leaf surface is defined as the rms value of the displacement.
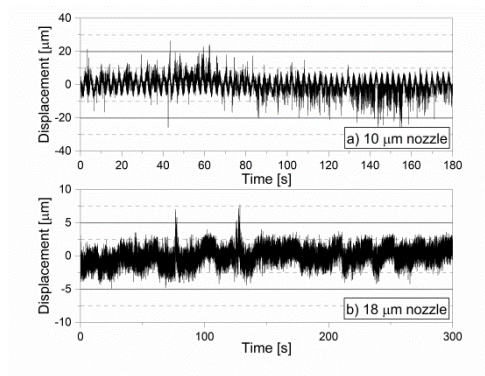

Figure 3. Measurement of the liquid leaf's position stability with a Micro-Epsilon® system. The leaf was produced with nozzles of (a) 10 μm and (b) 18 μm orifices, and a flowrate of 0.50 ml/ min and 1.27 ml/min, respectively.

As it is seen, the leaf produced with the smallest orifice is less stable than that produced with the largest one. The periodic variation of displacement is probably due to the flow dynamics. With an increasing flowrate the system shows better stability (Fig. 4.). In the most stable case, the mean value of displacement decreases to 0.99 and 1.33 μm for 10 and 18 μm orifice sizes, respectively.
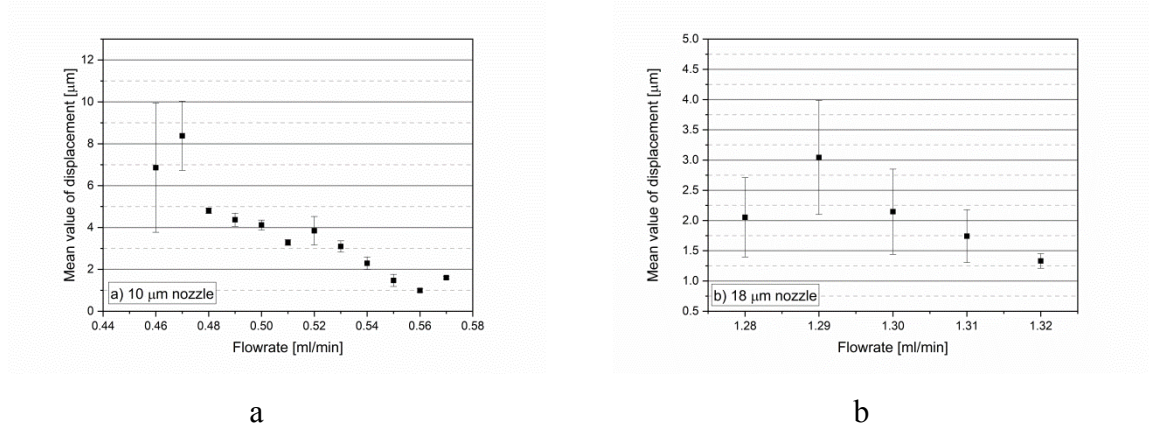
Figure 4. The mean value of displacement as a function of the flowrate for orifice sizes of 10 μm (a) and 18 μm (b). The error bar represents the standard deviaton of three independent measurements.

This natural uncertainty of the liquid jet system defines the maximum numerical aperture (N. A.) at which the target stays within the Rayleigh range of a Gaussian laser beam. Assuming laser pulses with a central wavelength of 850 nm, the maximum numerical apertures are shown in Table 1.

Flowrate [ml/min]	1.28	1.29	1.30	1.31	1.32
Displacment [μm]	2.05	3.04	2.14	1.74	1.33
N. A.	0.73	0.59	0.71	0.79	0.90

a.

Flowrate [ml/min]	0.46	0.47	0.48	0.49	0.50	0.51	0.52	0.53	0.54	0.55	0.56	0.57
Displacement [μm]	6.86	8.38	4.80	4.37	4.12	3.28	3.84	3.09	2.29	1.47	0.99	1.60
N. A.	0.39	0.36	0.47	0.50	0.51	0.57	0.53	0.59	0.68	0.85	1.04	0.82

b.

Table 1. The largest possible numerical aperture of a focusing element that can be used for focusing the laser pulse on the liquid leaf, under which the leaf stays within the Rayleigh range, as a function of the flowrate for an orifice of (a) 18 μm and (b) 10 μm in diameter.

As the table shows, there is a range of flowrates at which the liquid leaf stays stable. Once the flowrate is too low, the leaf collapses. At high flowrates, however, the liquid starts flicking at the collision point, making the leaf unstable again. For our microjets, the optimum flowrate is between 0.46 to 0.57 ml/min and 1.28 to 1.32 ml/min in case of 10 μm and 18 μm nozzle orifices, which supports our ion acceleration focusing power of N.A.=0.25. Therefore, in the following sections we investigate the liquid leaf properties within these flowrate regimes.

Resonant position stability

Besides the stochastic behavior of the flow dynamics of the colliding microjets, the position stability of the liquid leaf may also be affected by the laser interaction [22]. When the laser pulse impacts the leaf surface, part of it is absorbed and creates plasma. Upon this process, the flow is locally broken, which changes the flow dynamics of the leaf. As a result, the combined process of light absorption and flow break may result in a slight push of the leaf's position. When shooting laser pulses at a certain repetition rate, the periodic push of the leaf, regarded also as a certain type of pendulum, may make it swing. If the period of the swing happens to be close to the resonance of the leaf, the displacement of the leaf can besignificantly larger than the natural uncertainty of the sheet.

The effect of the periodic interaction of laser pulses on the liquid leaf was measured with the TeWaTi laser system of the University of Szeged [45]. The pulse energy and focal spot diameter were 50 mJ and 30 μm, respectively. The repetition rate of the laser pulses reaching the leaf was varied between 3 Hz to 100 Hz with a fast mechanical shutter before the power amplifier of the 100 Hz laser system. Fig. 5 shows the measured position error of the liquid leaf as a function of the pulse's repetition rate.
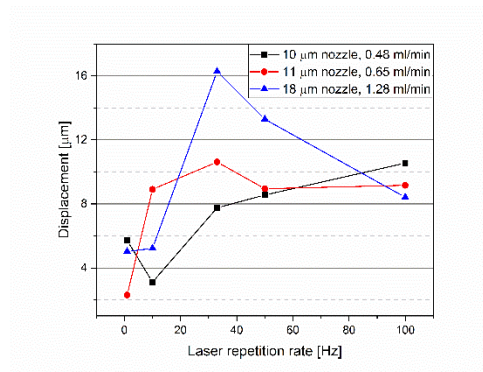
Figure 5. Displacement of the liquid sheet generated by periodic laser pulses for various orifice sizes as a function of the laser's repetition rate. (The lines are only to guide the eye.)

It can be seen that the periodic force of the laser pulses shows a clear resonance peak at 33 Hz in case of the largest orifice. For the smaller ones, the displacement flattens at around 10 μm towards the higher repetition rates. The displacement induced by the natural uncertainty mentioned above, and the laser pulse is still within the Rayleigh range of our N.A.=0.25 focusing element.

IV.　Experimental method and setup to measure nanometric transparent sheets

To develop a liquid leaf target with an intended thickness of hundreds of nanometers in vacuum, it is inevitable to implement a thickness measurement arrangement operational also in vacuum and providing the appropriate resolution. We chose a novel embodiment of classical spectral interferometry with broadband light sources. The thickness of the ultrathin sheet is determined from the period of spectral modulation appearing either in the reflection or in the transmission spectrum. The method highly depends on the accuracy of the spectral measurement of both the interference and the light source itself. After a comparative experimental study, we concluded that the measurement of transmittance is superior to that of reflectance, due to the accuracy of the measurement of the fundamental spectra.

In the case of submicron thick liquid sheets, the peaks and valleys in the spectral transmittance appear in the UV spectral range and at the lower end of the visible spectrum. This means that the liquid sheet must be illuminated by a light source with a sufficiently broad spectrum. Therefore, we use a combined deuterium and tungsten halogen lamp (*Ocean Insight, DH-2000-S-DUV*). To produce a flexible measurement system with good spatial resolution, optical fibers are used. The light beam of the combined lamp launched into a multimode UV-VIS fiber propagates through a flange using a simple mechanical coupling into another multimode fiber of the same type (Fig. 6). In the vacuum chamber a UV fused silica lens images the output of the optical fiber into a light spot of 50 μm on the liquid jet sheet. The distance between the lens and the sheet was 60 mm. The angle of incidence was always around 30 degree. In each case, the precise value was measured with the law of cosines.The light beam transmitted through the liquid jet sheet is imaged

by another fused silica lens into the input of another multimode UV-VIS optical fiber. Then the transmitted light beam goes through the flange again where the light is coupled into the last multimode fiber attached to a UV-VIS spectrometer (*Ocean Insight, FLAME-T-UV-VIS-ES*). At the beginning of each measurement, the liquid sheet was removed from the light paths, so that a reference spectrum of the input beam could be recorded.
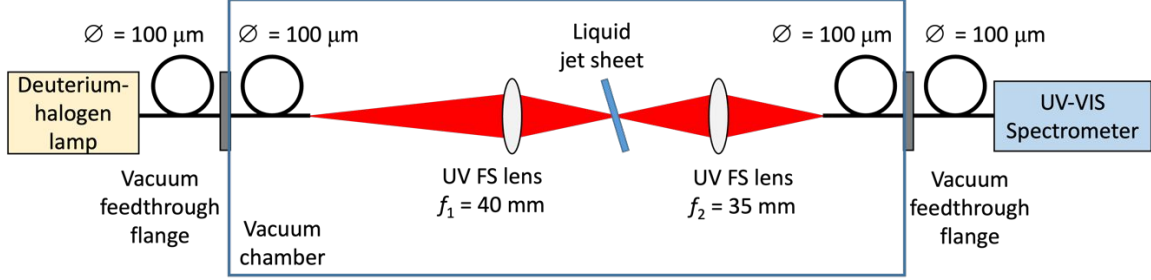

Figure 6. Schematic of the optical arrangement for thickness measurement in vacuum ambient operation (top view).

The spectral transmittance of the liquid sheet is formed by the interference among the directly transmitted beam and the beams reflected on the front and back surfaces of the sheet. In this way transmittance can be described by the multiple-beam interference formula as[46]:

$$\frac{I^{(t)}}{I^{(i)}} = \frac{1}{1 + F\sin\left(\frac{2\pi}{\lambda}n_2 h\cos\theta_2\right)^2}, \tag{1}$$

where $I^{(i)}$ and $I^{(t)}$ are the intensities of the input and the transmitted beams, respectively. λ is the wavelength, n_2 is the refractive index of the liquid sheet, θ_2 is the refraction angle, and h is the geometrical thickness of the sheet. The F parameter is defined as $4R/(1-R)^2$ with $R = \frac{(r_S^2 + r_P^2)}{2}$, where r_S and r_P are the reflection coefficients for s- and p-polarized light beams, which are determined by the Fresnel formulae as [46]:

$$r_p = \frac{n_2\cos\theta_1 - n_1\cos\theta_2}{n_1\cos\theta_2 + n_2\cos\theta_1}, \qquad r_s = \frac{n_1\cos\theta_1 - n_2\cos\theta_2}{n_1\cos\theta_1 + n_2\cos\theta_2}, \tag{2}$$

where θ_1 is the angle of incidence on the sheet and n_1 is the refractive index of the medium surrounding the liquid sheet.

11

If the theoretical curve given by Eq. (1) is fitted to the measured spectral transmittance values, and n_2 and θ_1 are known – and θ_2 can be calculated – then there is only one fitting parameter, the h geometrical thickness of the layer to be determined. Here we assumed that the small illuminated part can be approximated as a parallel sheet. In this case, the method mentioned above can be applied to map the thickenss of the liquid sheet.

During the measurements, we realized that in some cases the maximum of the measured transmittance was somewhat smaller than 1, due to scattering losses caused by the optically imperfect surface of the sheet. Therefore, we introduced another fitting parameter, A, which allowed us to take this effect into account, thus improving the precision of the fit:

$$\frac{I^{(t)}}{I^{(i)}} = A(\lambda)\frac{1}{1 + F\sin\left(\frac{2\pi}{\lambda}n_2 h\cos\theta_2\right)^2} \cdot \qquad (3)$$
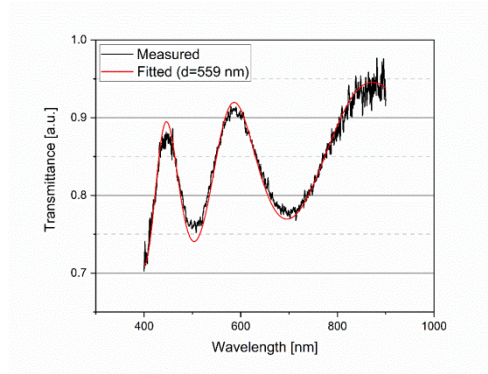

Figure 7. Measured spectral transmittance with the fitted curve of a PET foil.

The thickness measurement setup was first tested in air with a commercial, 0.5 μm thick polyester mylar (PET) foil. A piece of this material was strained to a rectangular holder to have a smooth enough sheet surface for measurement. With this transparent thin film, we could ensure the precise implementation of the system, and perform the first measurement. The standing target in air provided the simplest circumstances. A typical spectral transmittance is shown in Fig. 7 with the fitted curve. Here the scattering loss was wavelength dependent, unlike the liquid sheet. Therefore, in the fit function parameter A was not a simple constant, but the $A(\lambda) = \left(1 - \frac{C}{\lambda}\frac{1}{1-R}\right)^2$ expression was used, where C was a fitting parameter [46]. In the test measurement, we found that the PET foil was 559 nm thick, which was in good agreement with the expected value. The accuracy

of the measurement was ±2%, established as the rms error of five subsequent measurements.

V. Thickness measurement of the nanometric liquid sheet in air and in vacuum

After testing the systems, the thickness measurement setup and the liquid jet setup were installed on a vibration damped optical table (decoupled from the vacuum pumps) in the experimental chamber to characterize the liquid sheet target while varying its different parameters (see Fig. 1.a).

The critical parameter for ion acceleration experiments is the thickness of the liquid sheet. According to the Hasson-Peck model [43] the *h* thickness of a liquid sheet generated by two colliding liquid jets is given by:

$$h = \frac{d^2}{4r} \frac{sin^3\alpha}{(1 - cos\phi \, cos\alpha)^2} \tag{4}$$

where *d* is the diameter of the orifice of the nozzles, *r* is the radial distance from the point of impact, α is half of the impact angle and ϕ is the azimuthal angle. Although Eq. (4) provides the thickness, the formation of the layer is the result of different hydrodynamic effects, which can be influenced by many factors. Therefore, our aim was to measure the thickness of the liquid sheet in air and in vacuum.
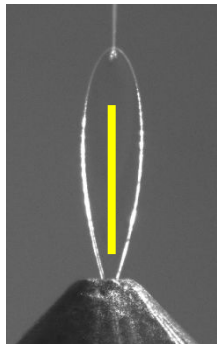
Thickness measurement in air

First, we examined how the thickness of the liquid leaf changes along its symmetry axis (yellow line in the insert image of Fig. 8 a) in air if the flowrate is varied. We used the collision point of the colliding round jets as the zero point of the vertical distances.

In Fig. 8 it can be seen that for all three flowrates the measured thicknesses follow the path of the theoretical curve given by Eq. (4). The thickness is inversely proportional to the distance measured from the reference point. We defined the starting point of the measurement, where the gradient of the leaf thickness variation was small enough compared to the measuring spot size, in order to maintain the visibility of the interference fringes.
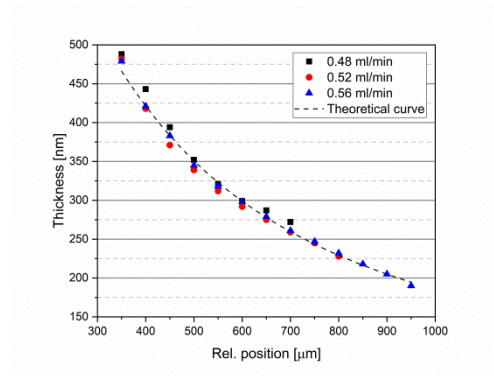
It is worth noting that the best theoretical fit provided slightly different collision angles, 54°, 50°, and 55° for 10 μm, 11 μm, and 18 μm orifices, respectively. The difference between the designed value and the real value of this angle originates from the mechanical properties of the glass-metal locking mechanism.

As seen, the higher the flowrate the longer the leaf is. Hence, the last measurable point is getting further away from the reference point. Because thickness is inversely proportional to distance, the increasing flowrate eventually results in a smaller thickness at the bottom end of the leaf. However, as Fig. 8c shows, the small thickness points possibly tend not to follow the prediction of the Hasson-Pech model as it is also seen in ref. [12, 25].
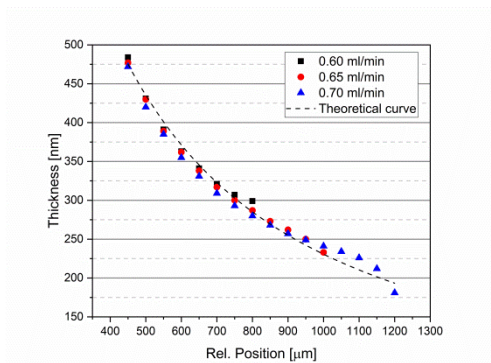
It is worth noting that the smallest thickness we measured was 182 nm. As it can be seen in Figure 8e, the fitting was still acceptable. We regard this measured value as the lowest end value of our measurement range. However, considering the experimental arrangement and the light source used, the ultimate limit would theoretically be around 100 nm.
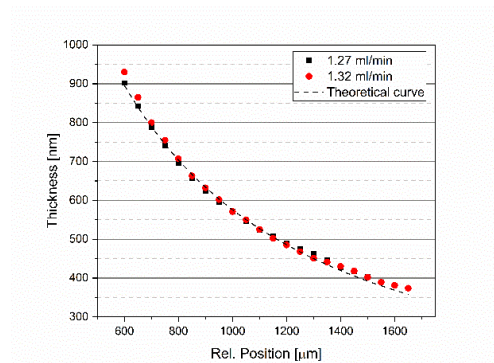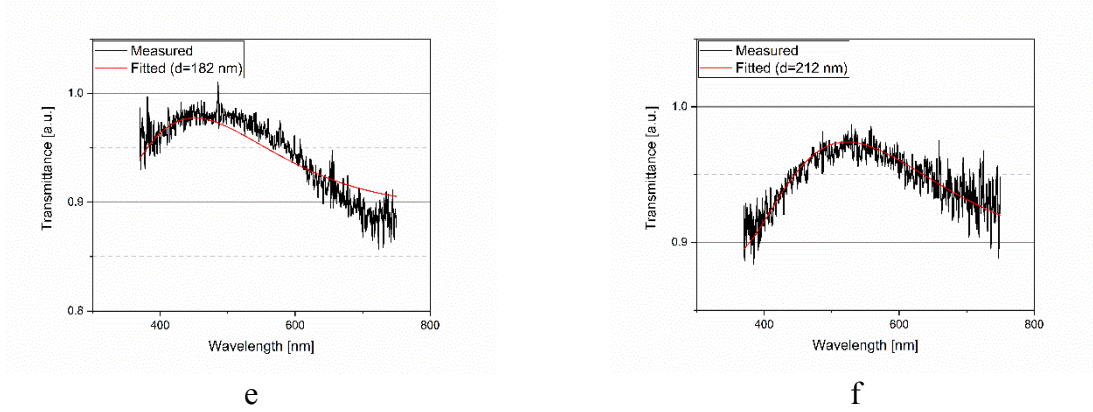

a

b

c

d

e   f

Figure 8. The thickness variation along the vertical axis (a) of the liquid leaf at different flowrates of water (orifice size: b) 10 μm c) 11 μm and d) 18 μm). The measured and evaluated spectral interference fringe is shown for the two thinnest values of 182 nm (e) and 212 nm (f). The error of the measurement was 3%.

To show the robustness of thickness tuning with position we measured the thickness in the full flowrate range at a few vertical positions (Fig. 9). The thickness was constant over the entire range with a measurement accuracy of 3% (the corresponding error bar is shown at the first measurement point of each series).
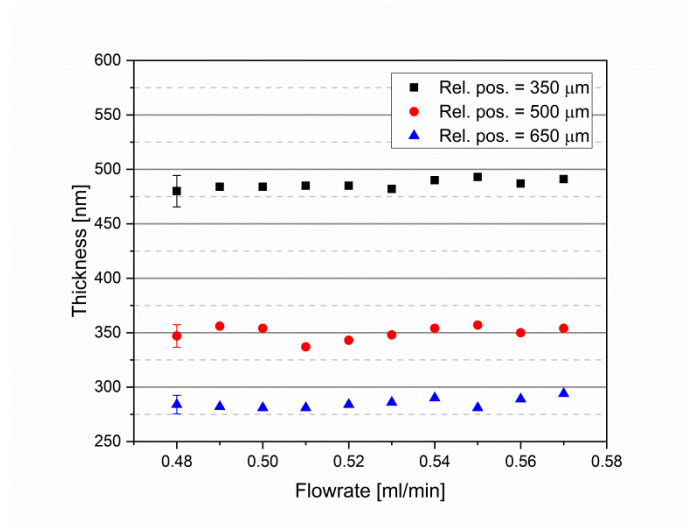

Figure 9. Thickness of the liquid leaf at a certain point on the vertical symmetry axis as a function of the flowrate (10 μm orifice size).

Previous measurements characterized the surface variation of the liquid leaf with the help of a monochromatic interference pattern [11, 20, 34-36]. To map the absolute thickness variation along the leaf, we measured the thickness of the leaf along horizontal and vertical lines point by point (dots in Fig. 10). As seen, all the measured points lie on the calculated theoretical surface. It is clear that the target is the thickest in the middle, on the

vertical symmetry axis, and its thickness decreases on both sides towards the visible rim around it (not presented on the surface plot). It is interesting to note that this description of thickness variation may provide a tool for finding the best position for laser-plasma ion acceleration.
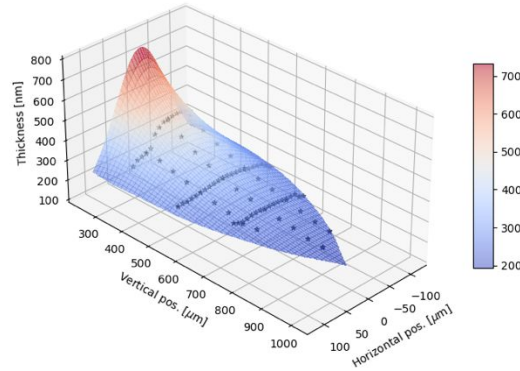

Figure 10. Grid of the measured thicknesses (stars) lying on the calculated thickness profile of the liquid leaf (10 μm orifice size and 0.54 ml/min flowrate

Thickness measurement in vacuum

The ultimate aim to accelerate ions from an ultrathin liquid jet in vacuum requires a pressure below 10^{-4} mbar. Existing data on the change of liquid leaf thickness in vacuum are contradictionary [12, 20]. Hence, after the liquid jet was characterized in the interaction chamber in air, a similar characterization process needs to be repeated in vacuum. To keep the liquid jet alive, a special evacuation protocol was developed. While we varied the the pumping speed, at a pressure of mbar level we started filling up the cold finger with liquid nitrogen untilthe ultimate vacuum was reached.

The evacuation process of the vacuum chamber did not affect the interferometric setup, which allowed us to examine the effect of the decreasing pressure on the leaf thickness. The thickness of the water sheet from the 11 μm orifice size was measured at a given point of the symmetry axis at a flowrate of 0.7 ml/min upon the evacuation process lasting

for 15–20 min (Fig. 11). As it is seen, the thickness of the layer decreases with falling pressure.
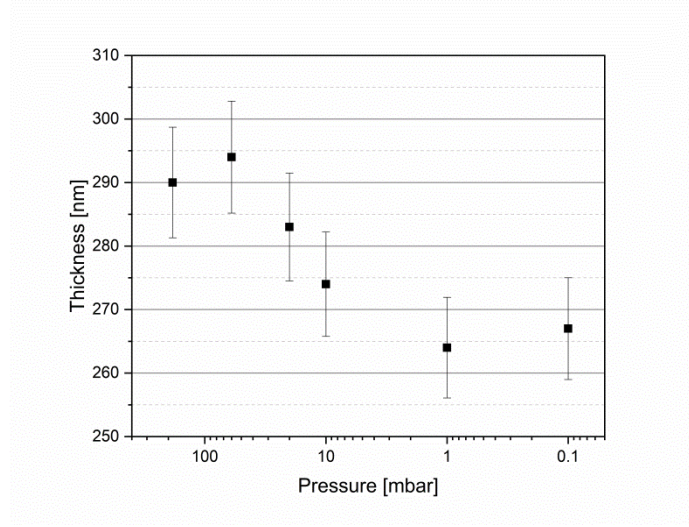

Figure 11. The thickness variation with the ambient pressure at a given point of the symmetry axis of the liquid leaf at a flowrate of 0.7 ml/min.

At the ultimate vacuum pressure of 10^{-4} mbar, the thickness of the sheets generated with 10 μm and 18 μm orifice size jets were scanned along the symmetry axis (Fig. 12). The shape of the measured curves was similar in both cases, however, the thickness values obtained in vacuum were 10% smaller than those obtained in air, confirming the measurement performed upon the evacuation process (Fig. 11). We think that the change in surface tension and the intense liquid evaporation in vacuum ultimately result in the thinning of the sheet.
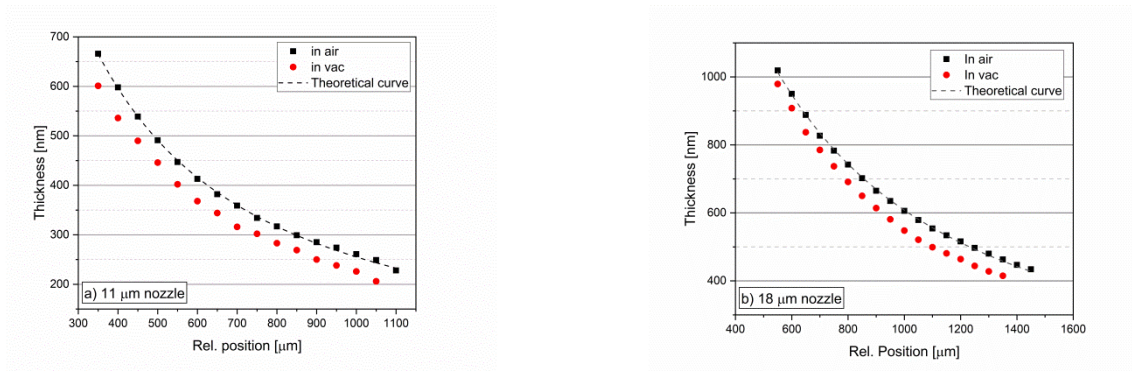

Figure 12. The measured thickness of the liquid sheet at a flowrate of 0.7 ml/min in air (black) and in vacuum (red) in case of 11 and 18 μm orifices

17

The stable liquid target must operate as long as it is possible for the long-term continuous generation of ions. Hence, we completed an endurance test in vacuum, too. For this purpose, we focused a diode laser (550 nm) beam gently onto the surface of the jet, and monitored the reflected beam position on a metal screen. From the geometry, we could calculate the position change of the spot and the rotation angle. Fig. 13 shows the results of the 200 min endurance test. During this long-term operation, the maximum detectable angle of rotation was around 76 mrad a few minutes after the start of the experiment. After the first 20 minutes, the system stabilized and from this point on the maximum rotation was less than 30 mrad. As a next step, we plan to further stabilize the rotation using an automatic control system.
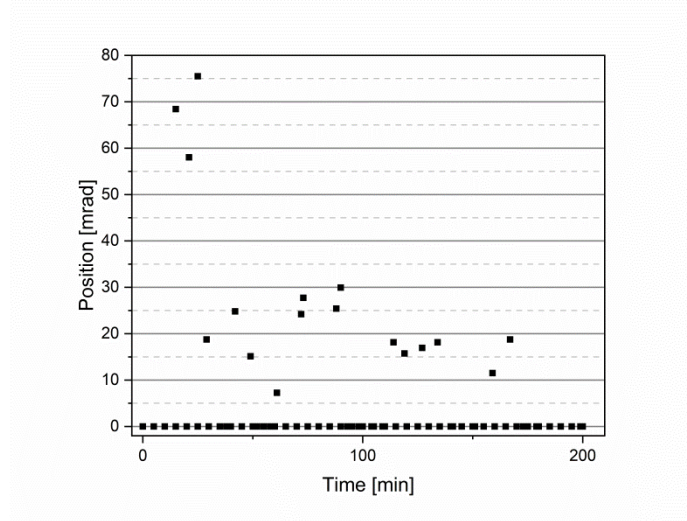

Figure 13. Endurance test results of the continuously working liquid jet. The data show the required rollback angle to the original direction of the liquid leaf, using the reflected light during the experiment.

VI.   Conclusions

We presented a liquid target system capable of continuous operation both in air and vacuum. Two microjets with round nozzles of 10, 11, and 18 μm in diameter collide creating an ultrathin layer of water sheet. The length and width of the liquid sheet, depending on the orifice size and the flowrate, is less than 1.5 mm and 0.4 mm, respectively. A catcher system, heated in vacuum and cooled in air, beneath the jets collects the liquid and helps recirculate the liquid. The position stability of the sheet is better than a few μm in the absence of laser pulses. Upon interaction with 50 mJ laser pulses at a repetition rate between 1 and 100 Hz, the 18 μm jet has a resonance amplitude

of 16 μm at a repetition rate of 33 Hz. Towards 100 Hz, the vibration amplitude of all three liquid sheets converges to 10 μm. This means that there are flowrates at each nozzle when the sheet position remains well within the Rayleigh range of the focusing optics up to a numerical aperture of 1.04. We have presented a method to measure the thickness of ultrathin liquid sheets in the interaction position within the vacuum chamber. The transmission white light spectral interference provides precise information on the liquid target's thickness under high vacuum conditions. The spot diameter was 50 μm, and the measurement range was 182 nm to 1 μm with an accuracy of ±3%. The position of the thinnest point of the liquid sheet depends on the distance from the top of the sheet as well as on the flowrate. In practice, this technique would allow for the tuning of the thickness of the liquid jet in two manners: either with the flowrate or the position of the liquid sheet with respect to the laser beam. The overall shape and 3D shape of the sheet are in good agreement with the Hasson-Peck model in air. In vacuum versus air, the sheet becomes gradually thinner by 10%, so the thinnest sheet achieved was below 200 nm at a vacuum level of 10^{-4} mbar, and remained stable for several hours of operation. This behavior with the possibility of infinite operation makes the developed liquid target an ideal target system for laser-based particle generation.

Acknowledgement

References:

1. S. Toth, T. Stanislauskas, I. Balciunas, R. Budriunas, J. Adamonis, R. Danilevicius, K. Viskontas, D. Lengvinas, G. Veitas, D. Gadonas, A. Varanavicius, J. Csontos, T. Somoskoi, L. Toth, A. Borzsonyi and K. Osvay, "SYLOS lasers–the frontier of few-cycle, multi-TW, kHz lasers for ultrafast applications at extreme light infrastructure attosecond light pulse source," *J. Phys. Photonics,* vol. 2, p. 045003, 2020.
2. C. Radier, O. Chalus, M. Charbonneau, S. Thambirajah, G. Deschamps, S. David, J. Barbe, E. Etter, G. Matras, S. Ricaud, V. Leroux, C. Richard, F. Lureau, A. Baleanu,

R. Banici, A. Gradinariu, C. Caldararu C. Capiteanu, H. Houe, M. Hebrat, H. Rocipon, A. Naziru, M. Risca, M. Merisanu, L. Caratas, B. Diaconescu, V. Iancu, R. Dabu, D. Ursescu, I. Dancus, C. A. Ur, K. A. Tanaka, and N. V. Zamfir, "10 PW peak power femtosecond laser pulses at ELI-NP," *High Power Laser Science and Engineering,* vol. 10, p. e21, 2022.

3. R. S. Nagymihaly, J. Bohus, V. Pajer, L. Lehotai, A. Malakzadeh, B. Bussiere, F. Falcoz, M. P. Khalashnikov, K. G. Varju, G. Szabo, C. Neacsu, P-M. Paul, G. Riboulet, A. Borzsonyi, "Operation experiences of the 10 Hz PW laser at ELI ALPS during the first ramping up phase," in *SPIE Conference on High-power, High-energy Lasers and Ultrafast Optical Technologies.*

4. T. Spinka, E. Sistrunk, A. Bayramian, J. P. Armstrong, S. Baxamusa, S. Betts, D. R. Bopp, S. Buck, K. Charron, J. Cupal, R. Demaret, R. Deri, J.-M. Di Nicola, A. Erlandson, E. S. Fulkerson, C. Gates, J. Horner, J. Horacek, J. Jarboe, K. Kasl, D. Kim, E. Koh, L. Koubikova, R. Lanning, J. Lusk, W. Maranville, C. Marshall, D. Mason, J. Menapace, P. Miller, P. Mazurek, A. J. Naylon, J. Nissen, J. Novak, D. Peceli, P. Rosso, K. Schaffers, T. Silva, D. Smith, J. Stanley, R. Steele, C. Stolz, T. Suratwala, S. Telford, J. Thoma, D. VanBlarcom, J. Weiss, P. Wegner, B. Rus, and C. Haefner, "Commissioning Results of the World's First Diode-Pumped 10Hz PW Laser," in *European Conference on Lasers and Electro-Optics and European Quantum Electronics Conference,,* 2017.

5. M. Faubel, B. Steiner, and J. P. Toennies, "Photoelectron spectroscopy of liquid water, some alcohols, and pure nonane in free micro jets," *J. Chem. Phys.,* vol. 106, p. 9013, 1997.

6. B. Winter and M. Faubel, "Photoemission from liquid aqueous solutions," *Chem. Rev.,* vol. 106, p. 1176, 2006.

7. D. Stemer, T. Buttersack, H. Haak, S. Malerz, H. Ch. Schewe, F. Trinter, K. Mudryk, M. Pugini, B. Credidio, R. Seidel, U. Hergenhahn, G. Meijer, S. Thürmer, and B. Winter, "Photoelectron spectroscopy from a liquid flatjet," *J. Chem. Phys.,* vol. 158, p. 234202, 2023.

8. T. Reuss, S. S. N. Lalithambika, Ch. David, F. Döring, Ch. Jooss, M. Risch, and S.Techert, "Advancements in Liquid Jet Technology and X-ray Spectroscopy for Understanding Energy Conversion Materials during Operation," *Acc. Chem. Res.,* vol. 56, p. 203, 2023.

9. P. Vester, I. Zaluzhnyy, Ruslan Kurta, K. B. Moller, E. Biasin, K. Haldrup,M. M. Nielsen, I. A. Vartanyants, "Ultrafast structural dynamics of photo-reactionsobserved by time-resolved x-ray cross-correlation analysis," *Struct. Dyn.,* vol. 6, p. 024301, 2019.

10. M. Fondell, S. Eckert, R. M. Jay, C. Weniger, W. Quevedo, J. Niskanen, B. Kennedy, F. Sorgenfrei, D. Schick, E. Giangrisostomi, R. Ovsyannikov, K. Adamczyk, N. Huse, P. Wernet, R. Mitzner, A. Föhlisch, "Time-resolved soft X-ray absorption spectroscopy in transmission mode on liquids at MHz repetition rates," *Structural Dynamics,* vol. 4, p. 054902, 2017.

11. J. D. Koralek, J. B. Kim, P. Brůža, Ch. B. Curry, Z. Chen, H. A. Bechtel, A. A. Cordones, P. Sperling, S. Toleikis, J. F. Kern, S. P. Moeller, S. H. Glenzer and D. P. DePonte, "Generation and characterization of ultrathin free-flowing liquid sheets," *Nat. Commun.,* vol. 9, p. 1353, 2018.

12. M. Ekimova, W. Quevedo, M. Faubel, P. Wernet and E. T. J. Nibbering, "A liquid flatjet system for solution phase soft-x-ray spectroscopy," *Struct. Dyn.,* vol. 2, p. 054301, 2015.

13. J. Snyder, J. Morrison, S. Feister, K. Frische, K. George, M. Le, C. Orban, G. Ngirmang, E. Chowdhury, W. Roquemore, "Background pressure effects on MeV protons accelerated via relativistically intense laser-plasma interactions," *Scientific Reports,* vol. 10, p. 18245, 2020.

14. S. Karsch, S. Düsterer, H. Schwoerer, F. Ewald, D. Habs, M. Hegelich, G. Pretzler, A. Pukhov, K. Witte, R. Sauerbrey, "High-Intensity Laser Induced Ion Acceleration from Heavy-Water Droplets," *Phys. Rev. Lett.,* vol. 91, p. 015001, 2003.

15. M. Schnürer, D. Hilscher, U. Jahnke, S. Ter-Avetisyan, S. Busch, M. Kalachnikov, H. Stiel, P. V. Nickles, W. Sandner, "Explosion characteristics of intense femtosecond-laser-driven water droplets," *Phys.Rev. E,* vol. 70, p. 056401, 2004.

16. J. B. Kim, S. Göde, S. H. Glenzer, "Development of a cryogenic hydrogen microjet for high-intensity, high-repetition rate experiments," *Rev. Sci. Instrum.,* vol. 87, p. 11E328, 2016.

17. M. Gauthier, C. B. Curry, S. Göde, F. -E. Brack, J. B. Kim, M. J. MacDonald, J. Metzkes, L. Obst, M. Rehwald, C. Rödel, H. -P. Schlenvoight, W. Schumaker, U. Schramm, K. Zeil, S. H. Glenzer, "High repetition rate, multi-MeV proton source from cryogenic hydrogen jets," *Appl. Phys. Lett.,* vol. 111, p. 114102, 2017.

18. L. Obst, S. Göde, M. Rehwald, F. -E. Brack, J. Branco, S. Bock, M. Bussmann, T. E. Cowan, C. B. Curry, F. Fiuza, M. Gauthier, R. Gebhart, U. Helbig, A. Huebl, U. Hübner, A. Irman, L. Kazak, J. B. Kim, T. Kluge, S. Kraft, M. Loeser, J. Mezkes, R. Mishra, C. Rödel, H. -P. Schlenvoigt, M. Siebold, J. Tiggesbaumker, S. Wolter, T. Ziegler, U. Schramm, S. H. Glenzer, K. Zeil, "Efficient laser-driven proton acceleration from cylindrical and planar cryogenic hydrogen jets," *Scientific Reports,* vol. 7, p. 10248, 2017.

19. J. T. Morrison, S. Feister, K. D. Frische, D. R. Austin, G. K. Ngirmang, N. R. Murphy, C. Orban, E. A. Chowdhury and W. M. Roquemore, "MeV proton acceleration at kHz repetition rate from ultra-intense laser liquid interaction," *New J. Phys.,* vol. 20, p. 022001, 2018.

20. G. Galinis, J. Strucka, J. C. T. Barnard, A. Braun, R. A. Smith, J. P. Marangos, "Micrometer-thickness liquid sheet jets flowing in vacuum," *Rev. Sci. Instrum.,* vol. 88, p. 083117, 2017.

21. C. J. Crissman, M. Mo, Z. Chen, J. Yang, D. A. Huyke, S. H. Glenzer, K. Ledbetter, J. P. F. Nunes, M. L. Ng, H. Wang, X. Shen, X. Wang and D. P. DePonte, "Sub-micron thick liquid sheets produced by isotropically etched glass nozzles," *Lab Chip,* vol. 22, p. 1365, 2022.

22. K. M. George, J. T. Morrison , S. Feister, G. K. Ngirmang , J. R. Smith , A. J. Klim , J. Snyder, "High-repetition-rate ($\geqslant$ kHz) targets and optics from liquid microjets for high-intensity laser–plasma interactions," *High Power Laser Science and Engineering,* vol. 7, p. e50, 2019.

23. M. Füle, T. Gilinger, B. G. Nagyillés, M. Karnok, P. Gaál, S. Figul, G. Marowsky, A. P. Kovács, K. Osvay, "Development of an ultrathin liquid leaf target system for deuteron acceleration at 10 Hz repetition rate," in *Laser Acceleration of Electrons, Protons, and Ions VII*, Praga, 2023.

24. F. Treffert C. B. Curry, H. -G. J. Chou, C. J. Crissman, D. P. DePonte, F. Fiuza, G. D. Glenn, R. C. Hollinger, R. Nedbalio, J. Park, C. Schoenwaelder, S. Song, S. Wang, J. J. Rocca, M. Roth, S. H. Glenzer, M. Gauthier, "High-repetition-rate, multi-MeV deuteron acceleration from converging heavy water microjets at laser intensities of 10^{21} W/cm^2," *Appl. Phys. Lett.,* vol. 121, p. 074104, 2022.

25. P. Puyuelo-Valdes, D. de Luis, J. Hernandez, J. I. Apiñaniz, A. Curcio, J. L. Henares, M. Huault, J. A. Pérez-Hernández, L. Roso, G. Gatti and L. Volpe, "Implementation of a thin, flat water target capable of high-repetition-rate MeV-range proton acceleration in a high-power laser at the CLPU," *Plasma Phys. Control. Fusion,* vol. 64, p. 054003, 2022.

26. Z. Cao, Z. Peng, Y. Shou, J. Zhao, S. Chen, Y. Gao, J. Liu, P. Wang, Z. Mei, Z. Pan, D. Kong, G. Qi, S. Xu, Z. Liu, Y. Liang, S. Xu, T. Song, X. Chen, Q. Wu, X. Liu, W. Ma, "Vibration and jitter of free-flowing thin liquid sheets as target for high-repetition-rate laser-ion acceleration," *Front. Phys.,* vol. 11, p. 1172075, 2023.

27. C. I. D. Underwood, G. Gan , Z.-H. He , C. D. Murphy, A. G. R. Thomas, K. Krushelnick, J. Nees , "Characterization of flowing liquid films as a regenerating plasma mirror for high repetitionrate laser contrast enhancement," *Laser and Particle Beams,* vol. 38, pp. 128-134, 2020.

28. E. d 'Humieres, E. Lefebvre, L.Gremillet, and V.Malka, "Proton acceleration mechanisms in high-intensity laser interaction with thin foils," *Phys. Plasma,* vol. 12, p. 062704, 2005.

29. T. Z. Esirkepov, M. Yamagiwa, and T. Tajima, "Laser Ion-Acceleration Scaling Laws Seen in Multiparametric Particle-in-Cell Simulations," *Phys. Rev. Lett.,* vol. 96, p. 105001, 2006.

30. M. Borghesi, A. Bigongiari, S. Kar, A Macchi, L. Romagnani, P. Audebert, J. Fuchs, T. Toncian, O. Willi, S V Bulanov, A .J. Mackinnon and J. C. Gauthier, "Laser-driven proton acceleration: source optimization and radiographic applications," *Plasma Phys. Control. Fusion,* vol. 50, p. 124040, 2008.

31. S. Steinke, A. Henig, M. Schnürer, T. Sokollik, P.V. Nickles, D. Jung, D. Kiefer, R. Hörlein, J. Schreiber, T. Tajima, X.Q. Yan, M. Hegelich, J. Meyer-ter-Vehn, W. Sandner and D. Habs, "Efficient ion acceleration by collective laser-driven electron dynamics with ultra-thin foil targets," *Laser and Particle Beams,* vol. 28, p. 215, 2010.

32. X.Q. Yan, T. Tajima, B.M. Hegelich, L. Yin, and D. Habs, "Theory of laser ion acceleration from a foil target of nanometer thickness," *Applied Phys. B,* vol. 98, p. 711, 2010.

33. S. Ter-Avetisyan, P. Varmazyar, P. K. Singh, J. G. Son, M. Fule, V. Yu. Bychenkov, B. Farkas, K. Nelissen, S. Mondal, D. Papp, A. Borzsonyi, J. Csontos, Zs. Lecz, T. Somoskoi, L. Toth, Sz. Toth, V. Andriy, D. Margarone, A. Necas, G. Morou, G. Szabo, K. Osvay, "Ion acceleration with few cycle relativistic laser pulses from foil targets," *Plasma Physics and Controlled Fusion,* vol. 65, p. 085012, 2023.

34. Y. J. Choo, B. S. Kang, " Parametric study on impinging-jet liquid sheet thickness distribution using an interferometric method," *Exp. In Fluids,* vol. 31, p. 56, 2001.

35. Y.-B-Shen, D. Poulikakos, "Thickness variation of a liquid sheet formed by two impinging jets using holographic interferometry," *Transactions of the ASME,* vol. 120, p. 482, 1998.

36. S. Menzi, G. Knopp, A. A. Haddad, S. Augustin, C. Borca, D. Gashi. T. Huthwelker, D. James, J. Jin, G. Pamfilidis, K. Schnorr, Z. Sun. R. Wetter, Q. Zhang, C. Cirelli, "Generation and somple charaterization of flat, liquid jets," *Rev. Sci. Instrum,,* vol. 91, p. 105109, 2020.

37. A. Watanabe, H. Saito, Y. Ishida, M. Nakamoto, T. Yajima, "A new nozzle producing ultrathin liquid sheets for femtosecond pulse dye lasers," *Opt. Commun.,* vol. 71, p. 301, 1989.

38. P. D. T. Huibers, D. O. Shah, "Multispectral determination of soap film thickness," *Langmuir,* vol. 13, p. 5995, 1997.

39. V. Bonal, J. A. Quintana, R. Muñoz-Mármol, J. M. Villalvilla, P. G. Boj, M. A. Díaz-García, "Sub-400 nm film thickness determination from transmission spectra in organic distributed feedback lasers fabrication," *Thin Solid Films,* vol. 692, p. 137580, 2019.

40. J. C. Manifacier, J. Gasiot and J. P. Fillard, "A simple method for the determination of the optical constants n, h and the thickness of a weakly absorbing thin film," *J. Phys. E: Sci. Instrum. ,* vol. 9, pp. 1002-1004, 1976.

41. Z. Yin, T.T. Luu, and H. J. Wörner, "Few-cycle high-harmonic generation in liquids: in-operando thickness measurement of flat microjets," *J. Phys. Photonics,* vol. 2, p. 044007, 2020.

42. G.Taylor, "Formation of Thin Flat Sheets of Water," *Proc. R. Soc. London. Ser A,* vol. 1296, p. 259, 1960.

43. D. Hasson, R. E. Peck, "Thickness distributionin a sheet formed by impinging jets," *AIChE J,* vol. 10, p. 752, 1964.

44. K. Osvay, M. Füle, T. Gilinger, B. Kis, P. K. Singh, S. Ter-Avetisyan, P. Varmazyar, B. Biró, L. Csedreki, Zs. Dombrádi, Z. Elekes, A. Fenyvesi, Zs. Fülöp, Z. Halász, Z. Korkulu, I. Kuti, L. Stuhl, "Deuteron acceleration and fast neutron generation with few-cycle, relativistic laser pulses at 1 Hz repetition rate," in *Laser Acceleration of Electrons, Protons, and Ions VII*, Praga, 2023.

45. P. Gaál, B. G. Nagyillés, M. Karnok, A. P. Kovács, T. Gilinger, M. Füle, Cs. Király, R. Nagymihaly, I. Seres, Sz. Tóth, K. Osvay, "A Variable Output 100 Hz Laser System With Few-cycle and TW Pulses," in *the European Conference on Lasers and Electro-Optics*, Munich, 2023.

46. M. Born, E. Wolf, in *Principles of Optics 7th. ed. Ch. 7.6.,*, Cambridge University Press, 2019.